ADVANCED MATERIALS
www.advmat.de

Robust Molecular Anodes for Electrocatalytic Water Oxidation Based on Electropolymerized Molecular Cu Complexes

Sebastian Amthor, Koushik Ranu, Carlos G. Bellido, Fernando F. Salomón, Alberto Piccioni, Raffaello Mazzaro, Federico Boscherini, Luca Pasquini, Marcos Gil-Sepulcre, and Antoni Llobet**

A multistep synthesis of a new tetra-amidate macrocyclic ligand functionalized with alkyl-thiophene moieties, 15,15-bis(6-(thiophen-3-yl)hexyl)-8,13-dihydro-5H-dibenzo[b,h][1,4,7,10]tetraazacyclotridecine-6,7,14,16(15H,17H)-tetraone, H_4L, is reported. The reaction of the deprotonated ligand, L^{4-}, and Cu(II) generates the complex $[LCu]^{2-}$, that can be further oxidized to Cu(III) with iodine to generate $[LCu]^{-}$. The H_4L ligand and their Cu complexes have been thoroughly characterized by analytic and spectroscopic techniques (including X-ray Absorption Spectroscopy, XAS). Under oxidative conditions, the thiophene group of $[LCu]^{2-}$ complex polymerizes on the surface of graphitic electrodes (glassy carbon disks (GC), glassy carbon plates (GC_p), carbon nanotubes (CNT), or graphite felts (GF)) generating highly stable thin films. With CNTs deposited on a GC by drop casting, hybrid molecular materials labeled as GC/CNT@p-$[LCu]^{2-}$ are obtained. The latter are characterized by electrochemical techniques that show their capacity to electrocatalytically oxidize water to dioxygen at neutral pH. These new molecular anodes achieve current densities in the range of 0.4 mA cm^{-2} at 1.30 V versus NHE with an onset overpotential at ≈250 mV. Bulk electrolysis experiments show an excellent stability achieving TONs in the range of 7600 during 24 h with no apparent loss of catalytic activity and maintaining the molecular catalyst integrity, as evidenced by electrochemical techniques and XAS spectroscopy.

1. Introduction

Water splitting with sunlight is among the most promising strategies at present that can potentially contribute to the urgently needed transition of fossil to solar fuels, in the short to medium term. To achieve this, efficient and robust catalysts both for the oxidation of water to molecular oxygen and the reduction of protons to hydrogen are necessary.[1–7] Further, in order to incorporate them into useful technological devices it is highly desirable to anchor them into conductive and/or semiconductive surfaces.[8–15] The development of water oxidation catalysts (WOCs) has followed two different strategies involving oxides[16–22] and molecular transition metal complexes.[23–26] For the latter case, highly performant and robust catalysts have been developed based on Ru complexes containing the so-called FAME (flexible, adaptable, multidentate, equatorial) ligands that achieve turnover numbers (TONs) in the range of millions and turnover frequency (TOF) in

S. Amthor, K. Ranu, C. G. Bellido, F. F. Salomón, M. Gil-Sepulcre, A. Llobet
Institute of Chemical Research of Catalonia (ICIQ)
Barcelona Institute of Science and Technology (BIST)
Avinguda Països Catalans 16, Tarragona 43007, Spain
E-mail: mgil@iciq.es; allobet@iciq.cat

The ORCID identification number(s) for the author(s) of this article can be found under https://doi.org/10.1002/adma.202308392

DOI: 10.1002/adma.202308392

A. Piccioni, R. Mazzaro, F. Boscherini, L. Pasquini
Department of Physics and Astronomy
Alma Mater Studiorum – Università di Bologna
viale C. Berti Pichat 6/2, Bologna 40127, Italy

A. Llobet
Departament de Química
Universitat Autònoma de Barcelona
Cerdanyola del Vallès, Barcelona 08193, Spain

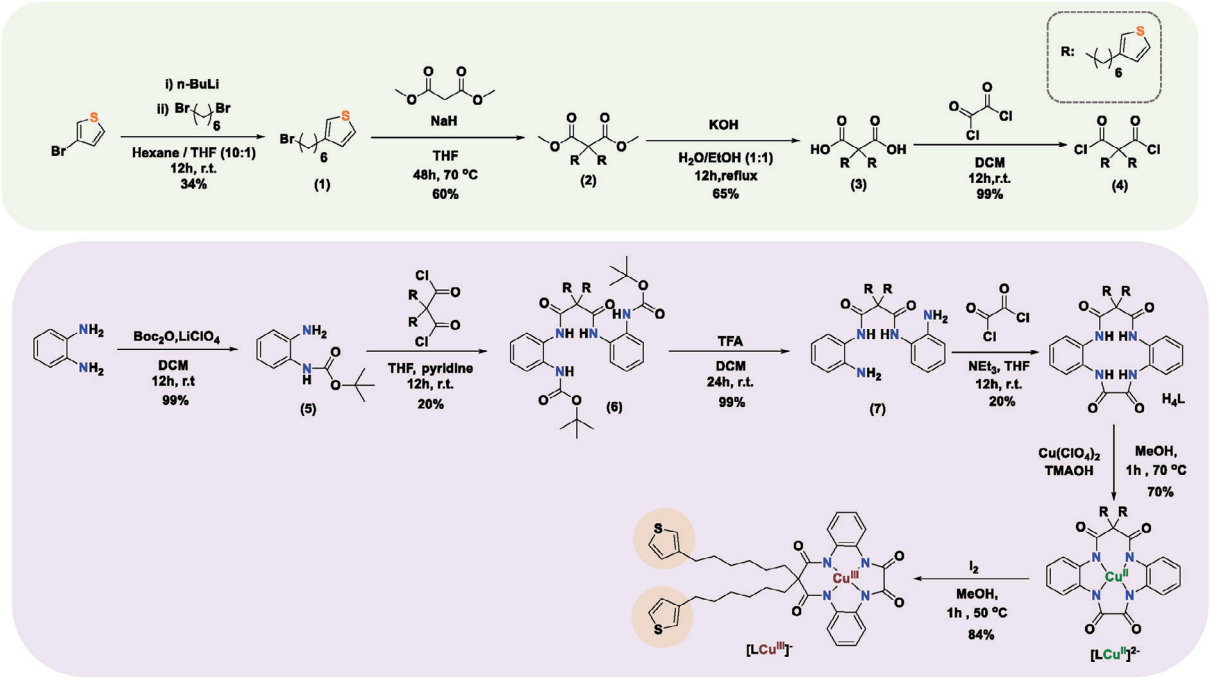

Scheme 1. Synthetic strategy followed for the preparation of the H_4L ligand and its Cu(II) and Cu(III) complexes **[LCu]**$^{2-}$ and **[LCu]**$^{-}$ respectively.

the microsecond timescale.[27–32] Given the scarcity of Ru in the earth's crust, it is mandatory to develop complexes that display similar performances based on first-row transition metals.[33–37] Unfortunately, most of the activities toward water oxidation that have been reported for first-row transition metal complexes are actually due to their transformation into the corresponding oxides.[38–40] The **[LCu]**$^{2-}$ (where the H_4L ligand is 15,15-bis(6-(thiophen-3-yl)hexyl)-8,13-dihydro-5H-dibenzo[b,h][1,4,7,10]tetraazacyclotridecine-6,7,14,16(15H,17H)-tetraone) complex stands out among one of the scarce number of complexes whose activity has been unambiguously demonstrated to be molecular in nature, and that can work at pH 7.[41–43]

Given the robustness displayed by the **[LCu]**$^{2-}$ as a WOC, we decided to develop a homologue that could be anchored on conductive and/or semiconductive surfaces by placing a thiophene group at the macrocyclic ligand backbone without modifying the intrinsic electronic properties of the original metal center.

Here on we report the synthesis of 15,15-bis(6-(thiophen-3-yl)hexyl)-8,13-dihydro-5H-dibenzo[b,h][1,4,7,10]tetraazacyclotridecine-6,7,14,16(15H,17H)-tetraone, H_4L, ligand and its Cu(II) and Cu(III) complexes **[LCu]**$^{2-}$ and **[LCu]**$^{-}$ respectively together with electropolymerization on graphitic electrodes and their performance as a water oxidation catalyst.

2. Results and Discussion

2.1. Synthesis and Structure of the Ligand and Its Discrete Cu Complexes

The synthesis of the H_4L ligand is based on a versatile multistep strategy that uses 3-(6-bromohexyl)thiophene and phenylenediamine as starting materials in combination with malonyl and oxalyl chloride as depicted in **Scheme 1** with good to moderate yields. This ligand and all the isolated synthetic intermediates have been characterized with the usual analytic and spectroscopic techniques (see details in Figures S1–S18, Supporting Information). Figure S6 (Supporting Information) shows the aromatic zone of the ^{1}H-NMR spectrum of H_4L in dmso-d_6 together with their proton integration and assignment, that is keyed in Scheme 1.

Reaction of $Cu(OTf)_2$ and the tetra-deprotonated ligand L^{4-} generates the corresponding dianionic Cu(II) complex **[LCu]**$^{2-}$ in good yields. This complex is characterized by mass spectrometry, elemental analysis, UV–vis spectroscopy (Figure S17b, Supporting Information) and by electrochemical techniques as will be described below. The local structure around the metal center was studied by X-ray absorption spectroscopy (XAS) at the Cu K edge, including X-ray absorption near edge structure (XANES—**Figure 1**, top) and extended X-ray absorption fine structure (EXAFS—**Figure** 1, bottom). The XANES spectrum of **[LCu]**$^{2-}$ exhibits the absorption edge (point of maximum slope on the rising absorption coefficient) at about 8985 eV, matching very well the parent, non-thiophene substituted complex **[(Mac)Cu^{II}]**$^{2-}$.[41] This agreement confirms that the two complexes are characterized by the same Cu(II) oxidation state. For the sake of comparison, the XANES spectrum of the chemically oxidized counterpart **[(Mac)Cu^{III}]**$^{-}$ is clearly shifted to higher energy and shows an edge at about 8988 eV, compatible with higher oxidation state Cu(III).[44,45]

Furthermore, the detailed analysis of the EXAFS signal, shown in Figure S27 (Supporting Information) and in Figure 1 (bottom) as Fourier transform (FT-EXAFS) in real space, yields a Cu-N average distance of ≈1.88 Å (see Table S2, Supporting Information), which is compatible with the value of ≈1.90 Å previously

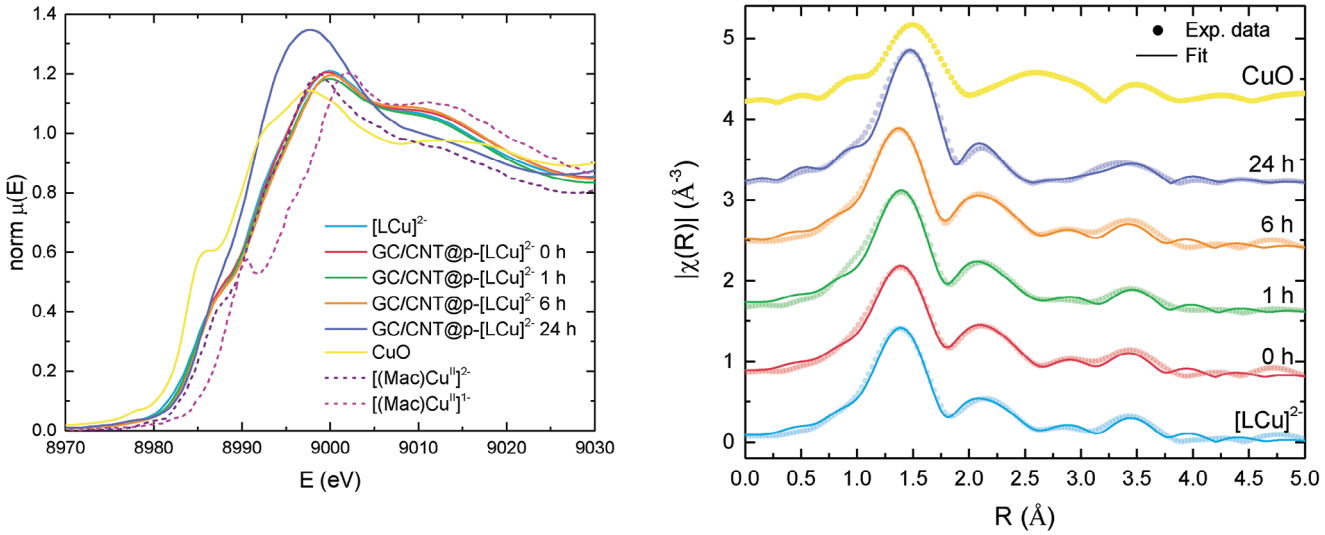

Figure 1. Top: normalized Cu K-edge XANES of **[LCu]**$^{2-}$ and electropolymerized **GC/CNT@p-[LCu]**$^{2-}$ both pristine (0 h) and after different CPE times under similar conditions as in Figure [4]: 1 h and roughly 316 TONs, 6 h and 1896 TONs, 24 h and 7600 TONs. The XANES spectra of the non-thiophene substituted counterpart **[(Mac)Cu^{II}]**$^{2-}$ and of its oxidized form **[(Mac)Cu^{III}]**$^{-}$ taken from our previous publication are also shown[41]. Bottom: Experimental Fourier transforms of k^2-weighted EXAFS spectra (dots) of **[LCu]**$^{2-}$ and electropolymerized **GC/CNT@p-[LCu]**$^{2-}$ samples, as above. The results of the fitting are represented as solid lines. See the Supporting Information for additional experimental details and quantitative analysis. The XANES and EXAFS spectra of a CuO reference sample are reported for the sake of comparison.

determined from the EXAFS analysis of the parent **[(Mac)Cu^{II}]**$^{2-}$ complex.[41] The two shoulders at ~8993 and ~8987 eV on the XANES edge can be assigned respectively to the transition to a 4p bound state and to a related transition with shakedown contribution, resulting from the concurrent ligand-to-metal charge transfer (LMCT).[45]

The d^8 diamagnetic Cu(III) complex **[LCu]**$^{-}$ is obtained using iodine as an oxidizing agent from the corresponding Cu(II) complex, **[LCu]**$^{2-}$, in good yields. This complex was characterized by 1D and 2D NMR spectroscopy and its ^{1}H-NMR spectrum in MeOH-d$_4$ is shown at the top of **Figure 2**. It is particularly interesting to compare the downfield shift of protons 1 and 4 of the phenylenediamine moiety as compared to the free ligand.

2.2. Electrochemical Polymerization and Spectroscopic Characterization

The electrochemical properties of the **[LCu]**$^{2-}$ monomer have been studied in acetonitrile based on cyclic voltammetry (CV) and differential pulse voltammetry (DPV) techniques. **Figure 3** (top) shows the CV of **[LCu]**$^{2-}$ in dry acetonitrile containing 0.1 M nBu$_4$PF$_6$ as supporting electrolyte, a Ag/Ag$^+$ (10 mM in MeCN) reference electrode and a glassy carbon (GC) as a working electrode. All potentials are converted to ferrocene by subtracting 110 mV.[46] A first reversible wave can be observed at $E_{1/2}$ = −0.45 V (grey and red trace) that is associated with the Cu(III/II) redox couple and agrees well with the similar potentials obtained for the **[(Mac)Cu]**$^{2-}$ complex previously reported. A second ill-defined wave with an anodic peak at ≈−0.15 V (red trace) is observed, that is associated with the Cu(III/II) couple of the monoprotonated complex **[HLCu]**$^{-}$. Addition of base completely suppresses this wave (blue trace, inset) indicating the existence of an equilibrium of these two species under the conditions studied here,

$$[\mathbf{LCu}]^{2-} + H^{+} -> [\mathbf{HLCu}]^{-} \quad (1)$$

Finally, a third wave at $E_{1/2}$ = 0.75 V is observed that is mainly associated with the oxidation of the thiophene moiety of the **[LCu]**$^{-}$ monomer. Surprisingly this oxidation does not lead to polymerization using nBu$_4$PF$_6$ as supporting electrolyte. However, using a mixture of 0.05 M nBu$_4$PF$_6$ and 0.05 NH$_4$TfO as supporting electrolyte it leads to electropolymerization as can be seen in Figure 3, bottom. The multiple cycling from −0.7 V up to 0.6 V of the **[LCu]**$^{2-}$ monomer in MeCN using a glassy carbon electrode containing multi-walled carbon nanotubes (**GC/CNT**; see Supporting Information for details) as a working electrode clearly shows a continuous increase of the current density as the multiple CVs are carried out. Further, as the polymerization proceeds, a new anodic wave appears at $E_{p,a}$ = 0.45 V, that is associated with the electroactivity of the polythiophene backbone. In this way a new molecular hybrid material is created, labelled as **GC/CNT@p-[LCu]**$^{2-}$. The area of the Cu(III/II) wave is used to calculate the amount of Cu catalyst deposited at the surface of the electrode that turns out to be of 50.4 μmol (Γ = 6.4 nmol cm^{-2}; see calculations in the Supporting Information).

Removing this electrode from the initial solution and placing it (after rinsing) in a neat MeCN electrolyte solution shows an electrochemical response that is practically identical to that of the 50th cycle (Figure S19, Supporting Information), indicating the stability of the electropolymerized complex in the CNT. To spectroscopically characterize this new material, we carried out XAS measurements following the same protocols as for **[LCu]**$^{2-}$. Both the XANES and the FT-EXAFS of **GC/CNT@p-[LCu]**$^{2-}$ (labelled **GC/CNT@p-[LCu]**$^{2-}$ **0 h** in Figure 1 to denote the pristine

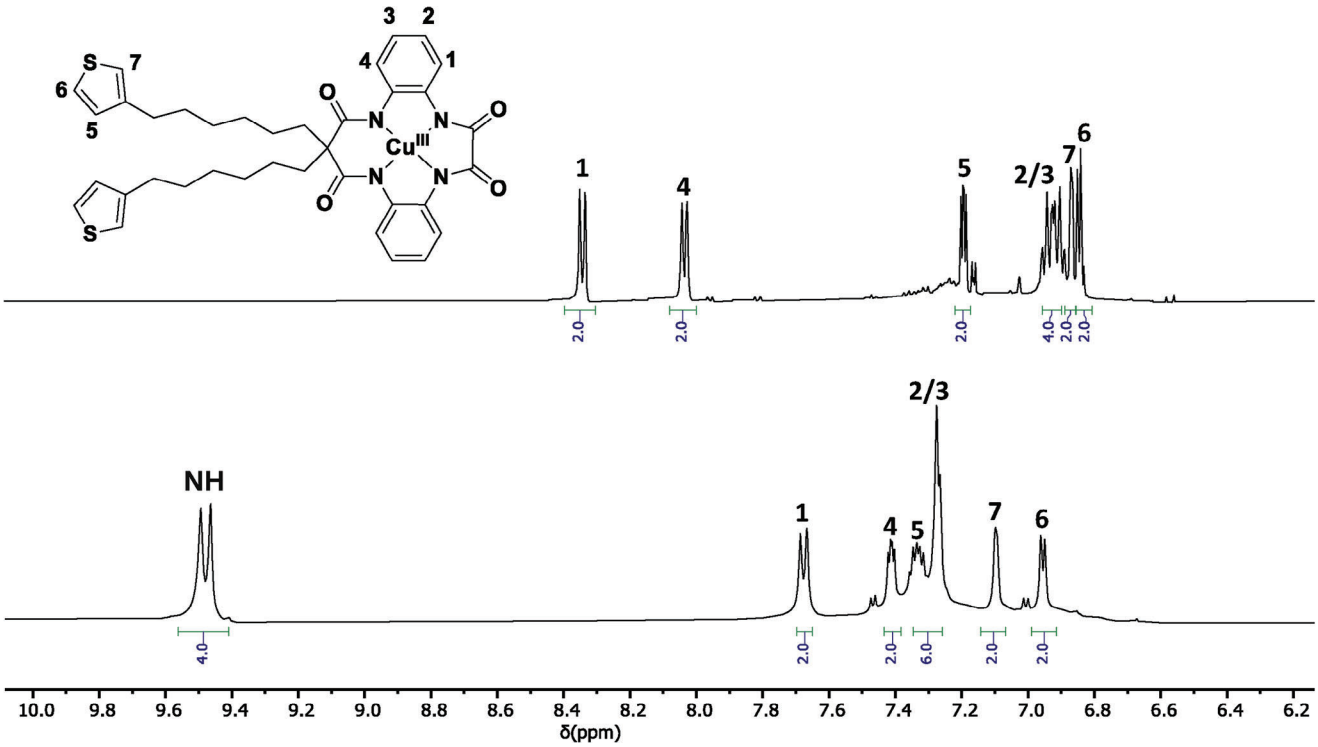

Figure 2. ^{1}H-NMR of complex **[LCu]**$^{-}$ (top) in MeOH-d_4 and ligand H_4**L** (bottom) in DMSO-d_6 at RT. Proton assignments are keyed in the drawn structure.

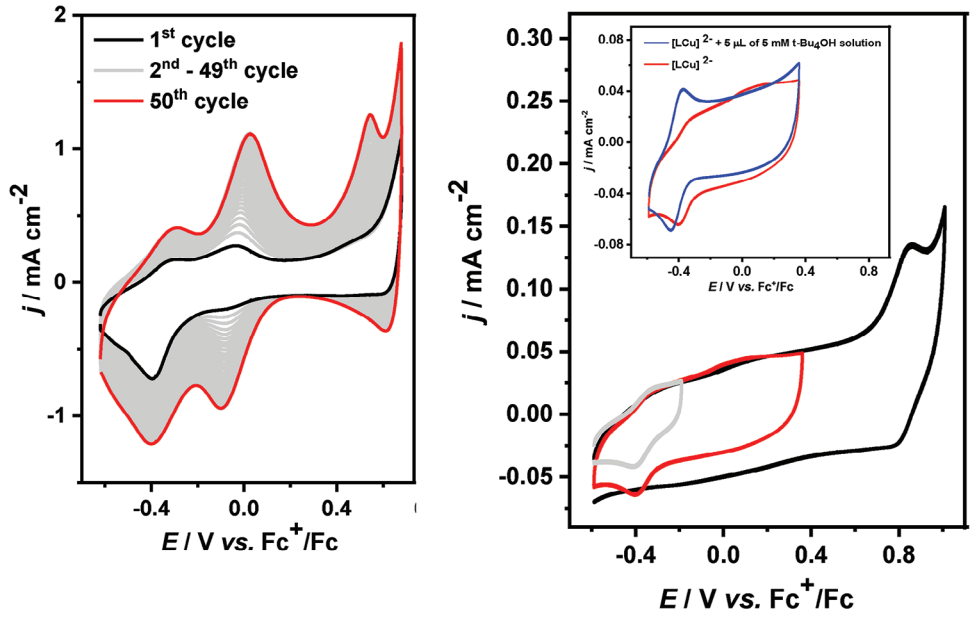

Figure 3. Top, CV of the monomer complex **[LCu]**$^{2-}$ in MeCN containing 0.1 M nBu$_4$PF$_6$ as supporting electrolyte at scan rate of 50 mV s^{-1} and using a GC disk as working electrode. Scanning anodically starting and finishing at −0.7 V and with a potential change versus ferrocene of: gray trace, E_c = −0.3 V; red trace, E_c = 0.25 V; black trace, E_c = 0.9 V. Inset, red trace same as in main graph; blue trace, after the addition of 5 µL of 5 mM solution of t-Bu$_4$OH. Bottom, 50 consecutive CV cycles (E_i = E_f = −0.6 V, E_c = 0.7 V) of a MeCN solution containing 3 mM **[LCu]**$^{2-}$ and a mixture of 0.05 M n-Bu$_4$PF$_6$ and 0.05 NH_4TfO as the supporting electrolyte at a scan rate of 50 mV s^{-1}, using a GC/CNT as a working electrode (see Supporting Information for details). Black trace, first CV cycle; red trace, 50th CV cycle; gray trace, intermediate cycles.

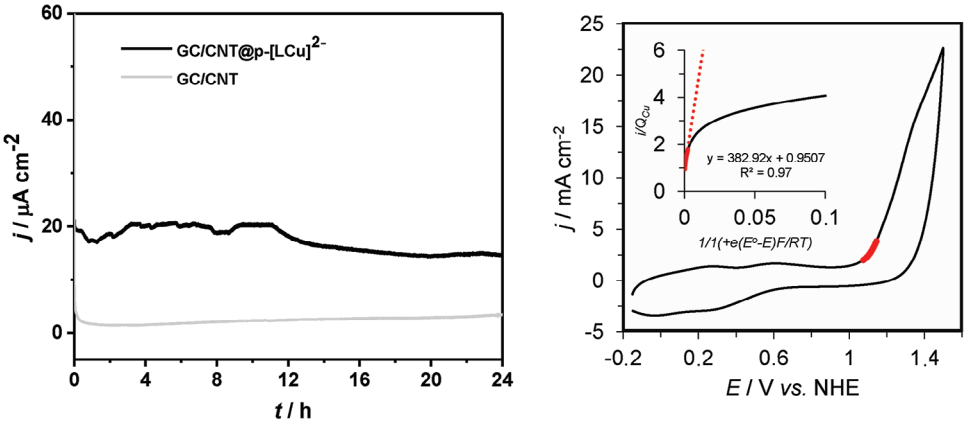

Figure 4. Top, CV of **GC/CNT@p-[LCu]**$^{2-}$ (Γ = 6.4 nmol cm^{-2}; size = 0.078 cm^2; 0.50 nmol of Cu) immersed in an aqueous phosphate buffer (0.1 M, pH 7) at a scan rate of 50 mV s^{-1}. Inset, FOWA region (obtained by plotting i/Q_{Cu} versus 1/{1+exp[(F(E−E°)/(RT)]}) for **GC/CNT@p-[LCu]**$^{2-}$. The black line corresponds to the experimental data used for FOWA analysis and red line shows the region used for the determination of k = TOF$_{max}$. Bottom, j versus t plot of a CPE experiment at E_{app} = 1.3 V for 24 h of **GC/CNT@p-[LCu]**$^{2-}$ (Γ = 6.4 nmol cm^{-2} of Cu) in an aqueous pH 7, 0.1 M phosphate buffer solution. Gray trace, background current from the GC/CNTs electrode under the same conditions. Charge, 1.48 C → 3.8 µmol of O_2 (assuming 100% Faradaic efficiency and 4 e− per O_2 molecule) implies a TON = 7600.

materials prior to electrocatalytic tests) are identical to those of the parent monomer **[LCu]**$^{2-}$, indicating that the oxidation state II of the metal center and its coordination environment do not change upon electropolymerization. This is further confirmed by the quantitative analysis reported in Table S2 (Supporting Information).

These new materials were further characterized by microscopy techniques including atomic force microscopy (AFM), scanning electron microscopy (SEM) and energy dispersive X-ray spectroscopy (EDX), being the results shown in Figure S25 (Supporting Information).

2.3. Catalytic Performance of Molecular Hybrid Materials GC/CNT@p-[LCu]$^{2-}$

The as prepared modified electrodes **GC/CNT@p-[LCu]**$^{2-}$ were tested toward water oxidation catalysis by immersing them into an aqueous 0.1 M phosphate buffer solution at pH 7. In aqueous solution a $Hg^0/HgSO_4$ (sat. K_2SO_4) reference electrode was used and the potentials are reported versus NHE by adding 0.65 V to the measured potential.[46] The resulting cyclic voltammogram is shown in **Figure 4**, top. The waves associated with the Cu(III/II) couples appeared at practically the same potential as in MeCN, although are wider, while the electroactivity of the polythiophene backbone is masked by a large electrocatalytic wave due to the oxidation of water to dioxygen, whose foot can be observed at ≈1.10 V. A Faradaic efficiency close to 100% was obtained via RRDE experiments that are describe in Figure S24 (Supporting Information). A kinetic analysis based on foot of the wave (FOWA) was also carried out (see the inset in Figure 4, left and additional details in the Supporting Information) giving a TOF$_{max}$ = 382 s^{-1} that compares well with the values reported in the literature in homogeneous phase for the parent complex **[(Mac)Cu]**$^{2-}$. In order to elucidate the long-term stability of the molecular hybrid material **GC/CNT@p-[LCu]**$^{2-}$, a controlled potential electrolysis (CPE) experiment at an E_{app} = 1.3 V was conducted for 24 h that is displayed in Figure 4, bottom. Once the potential is applied, a large number of bubbles appear that strongly adsorb at the surface of the electrode, decreasing its effective area. Under these conditions, a current of ≈20 µA cm^{-2} is generated that is practically maintained over 24 h, manifesting the robustness of this hybrid material. Overall, a total of 1.48 C was passed that involve 3.84 µmol of dioxygen that implies ≈7600 TONs, calculated according to measured Faradaic efficiency (100%).

To check the stability of the molecular hybrid material during the electrocatalytic process we carried out XAS on the hybrid materials after different CPE times (1, 6, and 24 h). Both the XANES and the FT-EXAFS measured after 1 and 6 h of CPE are almost identical to those of **[LCu]**$^{2-}$ and pristine **GC/CNT@p-[LCu]**$^{2-}$ **0 h**, indicating that the Cu(II) oxidation state and the local structure (coordination and interatomic distances) do not change. Differently, the XANES spectrum of sample **GC/CNT@p-[LCu]**$^{2-}$ **24 h** displays a blue shift of the absorption edge by ≈0.5 eV, together with a broadening of the white line, which embeds the pre-edge peak related to the 1s→4p transition. Even if a shift in the absorption energy suggests an increase of the oxidation state, the present energy shift is below the threshold indicated for the full transition from Cu(II) to Cu(III), usually in the range between 1 and 2 eV. In addition, the increase of the oxidation state in similar Cu complexes was previously directly correlated to an increase in the apparent ratio between the intensity of the LMCT-related transition and the 1s→4p transition, while the opposite trend is observed between the 24 h sample and the pristine complex.[45] Furthermore, comparing the FT-EXAFS spectra of **GC/CNT@p-[LCu]**$^{2-}$ **24 h** with pristine **[LCu]**$^{2-}$, we notice a shift of the first shell peak, corresponding to an expansion of the Cu-N nearest neighbor distance from ≈1.88 Å in **[LCu]**^{2} to ≈1.95 Å (see Table S2, Supporting Information). This contrasts with the idea of increased oxidation state, which should result in a contraction of the Cu–N distance. Therefore, it is more likely that the observed changes in XANES and EXAFS spectra arise from a distortion of the macrocyclic ligand rather than a change of oxidation state from Cu(II) to Cu(III). In addition, we can rule out the potential

deactivation pathway to CuO by looking at both the XANES and EXAFS spectra in Figure 1, which reveal a strong difference between CuO and all **GC/CNT@p-[LCu]**$^{2-}$ samples. In this regard, we remark that, apart from the first shell shift, the FT-EXAFS after 24 h of CPE is quite similar to the one of pristine **[LCu]**$^{2-}$, suggesting a good structural stability of the catalyst in harsh experimental conditions.

Additional tests with other graphitic materials were also carried out and the results are reported in the Supporting Information. It is interesting to mention here that when the catalyst is electropolymerized on the highly porous graphite felt (**GF**), high current densities of 0.4 mA cm^{-2} at 1.3 V are reached, yielding more than 11 000 TONs. A strategy to further increase current densities for potential applications, can involve the use of an even more porous material with a larger surface area together with increasing the amount of catalyst deposited at the electrode during the electropolymerization process.

3. Conclusions

The present work reports the creation of a molecular hybrid material labeled as **GC/CNT@p-[LCu]**$^{2-}$, containing a molecular Cu water oxidation catalyst. The molecular catalyst has been deposited at the surface of graphitic materials via oxidative electropolymerization of a thiophene group that had been previously introduced in the amide ligand backbone. This hybrid material represents the most robust molecular water oxidation catalysts anchored on a conductive surface based on a first-row transition metal, that maintains its integrity and activity over more than 11 000 TONs, as demonstrated by several techniques including XAS. Furthermore, this hybrid material works under neutral pH as opposed to most water oxidation catalyst based on Fe or Ni oxides that need to work under extremely basic pH. Moreover, the foot of the catalytic waves starts at ≈1.07 V that represents a very low overpotential of only 250 mV. The best molecular water oxidation catalysts based on Ru complexes with FAME ligands, present TONs over 1 million and TOFs in the range of 10^5 s^{-1} also at pH 7, but work at higher overpotentials around 450 mV.

The present work is the first example of a molecular water oxidation catalysts based on first row transition metal complex anchored on a conductive solid support, that maintains its molecular integrity after more than 11 000 TONs. This shows how the judicious use of the molecular toolkit allows to design and prepare oxidatively robust and long-lasting molecular hybrid materials, based on first row transition metals, for the electrocatalytic oxidation of water to dioxygen at low overpotentials. This work paves the way for the use of precious metal free hybrid materials as catalysts for electro- and photoelectrochemical water splitting devices, in the domain of solar fuels and more broadly in the solar to chemical products applications.

Supporting Information

Supporting Information is available from the Wiley Online Library or from the author.

Acknowledgements

S.A. and K.R. contributed equally to this work. This project has received funding from the European Union's Horizon 2020 research and innovation program under grant agreement No 101006839 (CONDOR). The authors acknowledge the European Synchrotron Radiation Facility (ESRF) for provision of synchrotron radiation facilities under proposal number A08-1-1078 and they would like to thank the staff of BM-08 LISA for excellent support. A.L. acknowledges financial support from Ministerio de Ciencia e Innovación through projects PID2022-140143OB-I00 and SO-CEX2019-000925-S (MCIN/AEI/10.13039/5011000110). K.R. acknowledges a FI AGAUR Fellowship ref: 2022 FI_B 00459 from Generalitat de Catalunya.

Conflict of Interest

The authors declare no conflict of interest.

Data Availability Statement

The data that support the findings of this study are available in the Supporting Information of this article.

Keywords

anchored molecular catalysts, first row transition metal complexes, redox catalysis, water oxidation catalysis

Received: August 18, 2023
Revised: September 17, 2023
Published online:

[1] P. Nejat, F. Jomehzadeh, M. M. Taheri, M. Gohari, M. Z. Abd. Majid, *Renewable Sustainable Energy Rev.* **2015**, *43*, 843.
[2] T. R. Cook, D. K. Dogutan, S. Y. Reece, Y. Surendranath, T. S. Teets, D. G. Nocera, *Chem. Rev.* **2010**, *110*, 6474.
[3] A. H. Proppe, Y. C. Li, A. Aspuru-Guzik, C. P. Berlinguette, C. J. Chang, R. Cogdell, A. G. Doyle, J. Flick, N. M. Gabor, R. Van Grondelle, S. Hammes-Schiffer, S. A. Jaffer, S. O. Kelley, M. Leclerc, K. Leo, T. E. Mallouk, P. Narang, G. S. Schlau-Cohen, G. D. Scholes, A. Vojvodic, V. W.-W. Yam, J. Y. Yang, E. H. Sargent, *Nat. Rev. Mater.* **2020**, *5*, 828.
[4] C. C. L. Mccrory, S. Jung, J. C. Peters, T. F. Jaramillo, *J. Am. Chem. Soc.* **2013**, *135*, 16977.
[5] K. Sun, I. A. Moreno-Hernandez, W. C. Schmidt, X. Zhou, J. C. Crompton, R. Liu, F. H. Saadi, Y. Chen, K. M. Papadantonakis, N. S. Lewis, *Energy Environ. Sci.* **2017**, *10*, 987.
[6] R. Matheu, P. Garrido-Barros, M. Gil-Sepulcre, M. Z. Ertem, X. Sala, C. Gimbert-Suriñach, A. Llobet, *Nat. Rev. Chem.* **2019**, *3*, 331.
[7] J. D. Blakemore, R. H. Crabtree, G. W. Brudvig, *Chem. Rev.* **2015**, *115*, 12974.
[8] Z. N. Zahran, Y. Tsubonouchi, E. A. Mohamed, M. Yagi, *ChemSusChem* **2019**, *12*, 1775.
[9] A. Vasileff, C. Xu, Y. Jiao, Y. Zheng, S.-Z. Qiao, *Chem* **2018**, *4*, 1809.
[10] M. Yamamoto, L. Wang, F. Li, T. Fukushima, K. Tanaka, L. Sun, H. Imahori, *Chem. Sci.* **2016**, *7*, 1430.
[11] J. T. Hyde, K. Hanson, A. K. Vannucci, A. M. Lapides, L. Alibabaei, M. R. Norris, T. J. Meyer, D. P. Harrison, *ACS Appl. Mater. Interfaces* **2015**, *7*, 9554.
[12] L. Francàs, C. Richmond, P. Garrido-Barros, N. Planas, S. Roeser, J. Benet-Buchholz, L. Escriche, X. Sala, A. Llobet, *Chemistry* **2016**, *22*, 5261.
[13] J. D. Blakemore, A. Gupta, J. J. Warren, B. S. Brunschwig, H. B. Gray, *J. Am. Chem. Soc.* **2013**, *135*, 18288.
[14] S. W. Sheehan, J. M. Thomsen, U. Hintermair, R. H. Crabtree, G. W. Brudvig, C. A. Schmuttenmaer, *Nat. Commun.* **2015**, *6*, 6469.

[15] M. Ventosa, M. Gil-Sepulcre, J. Benet-Buchholz, C. Gimbert-Suriñach, A. Llobet, *ACS Appl. Energy Mater.* **2021**, *4*, 9775.
[16] M. I. Díez-García, G. Montaña-Mora, M. Botifoll, A. Cabot, J. Arbiol, M. Qamar, J. R. Morante, *ACS Appl. Energy Mater.* **2023**, *6*, 5690.
[17] Y. Xu, K. Fan, Y. Zou, H. Fu, M. Dong, Y. Dou, Y. Wang, S. Chen, H. Yin, M. Al-Mamun, P. Liu, H. Zhao, *Nanoscale* **2021**, *13*, 20324.
[18] Y. Lee, J. Suntivich, K. J. May, E. E. Perry, Y. Shao-Horn, *J. Phys. Chem. Lett.* **2012**, *3*, 399.
[19] J. Melder, S. Mebs, F. Lessing, H. Dau, P. Kurz, *Sustainable Energy Fuels* **2023**, *7*, 92.
[20] F. Song, L. Bai, A. Moysiadou, S. Lee, C. Hu, L. Liardet, X. Hu, *J. Am. Chem. Soc.* **2018**, *140*, 7748.
[21] K. Azmani, M. Besora, J. Soriano-López, M. Landolsi, A.-L. Teillout, P. de Oliveira, I.-M. Mbomekallé, J. M. Poblet, J.-R. Galán-Mascarós, *Chem. Sci.* **2021**, *12*, 8755.
[22] B. M. Hunter, H. B. Gray, A. M. Müller, *Chem. Rev.* **2016**, *116*, 14120.
[23] P. Garrido-Barros, C. Gimbert-Suriñach, R. Matheu, X. Sala, A. Llobet, *Chem. Soc. Rev.* **2017**, *46*, 6088.
[24] M. D. Karkas, B. Akermark, *Dalton Trans.* **2016**, *45*, 14421.
[25] J. D. Blakemore, N. D. Schley, D. Balcells, J. F. Hull, G. W. Olack, C. D. Incarvito, O. Eisenstein, G. W. Brudvig, R. H. Crabtree, *J. Am. Chem. Soc.* **2010**, *132*, 16017.
[26] S. Berardi, S. Drouet, L. Francàs, C. Gimbert-Suriñach, M. Guttentag, C. Richmond, T. Stoll, A. Llobet, *Chem. Soc. Rev.* **2014**, *43*, 7501.
[27] M. Gil-Sepulcre, J. O. Lindner, D. Schindler, L. Velasco, D. Moonshiram, O. Rüdiger, S. DeBeer, V. Stepanenko, E. Solano, F. Würthner, A. Llobet, *J. Am. Chem. Soc.* **2021**, *143*, 11651.
[28] J. Creus, R. Matheu, I. Peñafiel, D. Moonshiram, P. Blondeau, J. Benet-Buchholz, J. García-Antón, X. Sala, C. Godard, A. Llobet, *Angew. Chem., Int. Ed.* **2016**, *55*, 15382.
[29] R. Matheu, M. Z. Ertem, C. Gimbert-Suriñach, X. Sala, A. Llobet, *Chem. Rev.* **2019**, *119*, 3453.
[30] B. Zhang, L. Sun, *J. Am. Chem. Soc.* **2019**, *141*, 5565.
[31] L. Duan, F. Bozoglian, S. Mandal, B. Stewart, T. Privalov, A. Llobet, L. Sun, *Nat. Chem.* **2012**, *4*, 418.
[32] R. Matheu, J. Benet-Buchholz, X. Sala, A. Llobet, *Inorg. Chem.* **2018**, *57*, 1757.
[33] M. Gil-Sepulcre, A. Llobet, *Nat. Catal.* **2022**, *5*, 79.
[34] L.-H. Zhang, S. Mathew, J. Hessels, J. N. H. Reek, F. Yu, *ChemSusChem* **2021**, *14*, 234.
[35] D. Den Boer, A. I. Konovalov, M. A. Siegler, D. G. H. Hetterscheid, *Inorg. Chem.* **2023**, *62*, 5303.
[36] A. M. Geer, C. Musgrave Iii, C. Webber, R. J. Nielsen, B. A. Mckeown, C. Liu, P. P. M. Schleker, P. Jakes, X. Jia, D. A. Dickie, J. Granwehr, S. Zhang, C. W. Machan, W. A. Goddard, T. B. Gunnoe, *ACS Catal.* **2021**, *11*, 7223.
[37] D. P. Adiyeri Saseendran, J. W. A. Fischer, L. Müller, D. F. Abbott, V. Mougel, G. Jeschke, C. A. Triana, G. R. Patzke, *Chem. Commun.* **2023**, *59*, 5866.
[38] P. Pelosin, M. Gil-Sepulcre, P. Garrido-Barros, D. Moonshiram, J. Benet-Buchholz, C. Gimbert-Suriñach, A. Llobet, *iScience* **2020**, *23*, 101378.
[39] S. J. Folkman, J. Soriano-Lopez, J. R. Galán-Mascarós, R. G. Finke, *J. Am. Chem. Soc.* **2018**, *140*, 12040.
[40] N. Kaeffer, A. Morozan, J. Fize, E. Martinez, L. Guetaz, V. Artero, *ACS Catal.* **2016**, *6*, 3727.
[41] P. Garrido-Barros, D. Moonshiram, M. Gil-Sepulcre, P. Pelosin, C. Gimbert-Suriñach, J. Benet-Buchholz, A. Llobet, *J. Am. Chem. Soc.* **2020**, *142*, 17434.
[42] P. Garrido-Barros, I. Funes-Ardoiz, S. Drouet, J. Benet-Buchholz, F. Maseras, A. Llobet, *J. Am. Chem. Soc.* **2015**, *137*, 6758.
[43] P. Garrido-Barros, C. Gimbert-Suriñach, D. Moonshiram, A. Picón, P. Monge, V. S. Batista, A. Llobet, *J. Am. Chem. Soc.* **2017**, *139*, 12907.
[44] L. S. Kau, D. J. Spira-Solomon, J. E. Penner-Hahn, K. O. Hodgson, E. I. Solomon, *J. Am. Chem. Soc.* **1987**, *109*, 6433.
[45] J. L. Dubois, P. Mukherjee, T. D. P. Stack, B. Hedman, E. I. Solomon, K. O. Hodgson, *J. Am. Chem. Soc.* **2000**, *122*, 5775.
[46] V. V. Pavlishchuk, A. W. Addison, *Inorg. Chim. Acta* **2000**, *298*, 97.